The Assimilation of Wind Speed and Direction Based on WRFDA 3D-Var System

Feng Gao[1,2], Xiang-Yu Huang[1], Neil A. Jacobs[3]

[1]National Center for Atmospheric Research, Boulder, Colorado, USA
[2] Nanjing University of Information Science & Technology, Nanjing, Jiangsu, China
[3]AirDat LLC, Morrisville, North Carolina, USA

1. Introduction

The present scheme for assimilating wind observations into the Weather Research and Forecasting Data Assimilation (WRFDA) three-dimensional variational data assimilation (3D-Var) system employs *u* and *v* wind vector components calculated from observed wind speed (*sp*) and wind direction (*dir*). Since aircraft, as well as other observation platforms, sample the environment in a *sp* and *dir* framework, these observations are converted to vector components, and then the observational errors of the *u* and *v* components are assigned based on the *sp* errors in the pre-processing of observations. The process does not consider the *dir* observational error. Once this conversion takes place, the ability to isolate the *dir* observational error as an independent source from the *sp* magnitude observational error is lost. Given this situation, the *dir* is assumed to be error-free, and the weight of analysis between background and observations will only be affected by the *sp* observational error, which can make impacts on both *sp* and *dir* components of the analysis. However, Gao et al. (2012) show that the observed *dir* has a unique, and often inversely proportional, error compared to *sp*, where large *dir* errors are encountered when *sp* is small. We hypothesize that the wind observation selection, rejection, and weighting can be refined if the *dir* observational error is considered in addition to *sp* prior to calculating the vector components of the observed wind. In order to test this hypothesis, a new method of directly assimilating *sp* and *dir* was introduced in WRFDA 3D-Var system.

The remainder of this paper describes the theory, code development and experimental results. In section 2, the observation operator and code development are introduced. Section 3 presents the differences of analysis between assimilating *u* and *v* winds (asm_uv) and assimilating *sp* and *dir* (asm_wind). A set of Observing System Simulation Experiments (OSSE) is presented in section 4. Conclusions and plans for future work are discussed in section 5.

2. The new formulation

The WRFDA variational data assimilation system is based on multivariate incremental formulation that is commonly used in operational system (Courtier et al. 1994; Huang et al. 2009). The prescribed cost function for 3D-Var system can be expressed as:

$$J(x) = J_b + J_o = \frac{1}{2}(x - x_b)^T B^{-1}(x - x_b) + \frac{1}{2}(y_o - H(x))^T R^{-1}(y_o - H(x)) \qquad (1)$$

After setting $\nabla J(x) = 0$ to ensure that $J(x)$ is a minimum, the solution of the cost function can be obtained :

$$x_a = x_b + \left(\mathrm{B}^{-1} + \mathrm{H}^{\mathrm{T}}\mathrm{R}^{-1}\mathrm{H}\right)^{-1} \mathrm{H}^{\mathrm{T}}\mathrm{R}^{-1}\left(y_o - H\left(x_b\right)\right) \qquad (2)$$

where B is the background error covariance matrix, R is the observation error covariance matrix, H is the linearized version of nonlinear operator H, the superscript T means the adjoint of this matrix, and the innovation vector (IV) is $y_0 - H(x_b)$.

2.1 Observation operator

The advantage of the variational scheme in Eq. (2) is its ability to efficiently assimilate various types of observations based on the nonlinear observation operator and its related tangent linear (TL) and adjoint operators (AD). The nonlinear observation operators (*H*) for *SP* and *DIR* are expressed as:

$$sp = (u^2 + v^2)^{1/2} \qquad dir = n\pi + \arctan(\frac{u}{v}) \tag{3}$$

where *u* and *v* are the wind vector components from the model first guess or background, and *n* is an integer used to adjust the wind direction quadrant. Using Eq. (3), we can express the TL process (y=H(x)) as:

$$\begin{pmatrix} \delta sp \\ \delta dir \end{pmatrix} = \begin{pmatrix} \frac{u}{\sqrt{u^2+v^2}} & \frac{v}{\sqrt{u^2+v^2}} \\ \frac{v}{u^2+v^2} & \frac{-u}{u^2+v^2} \end{pmatrix} \begin{pmatrix} \delta u \\ \delta v \end{pmatrix} \tag{4}$$

and the AD process ($x^*=H^T(y^*)$) as:

$$\begin{pmatrix} \delta^* u \\ \delta^* v \end{pmatrix} = \begin{pmatrix} \frac{u}{\sqrt{u^2+v^2}} & \frac{v}{u^2+v^2} \\ \frac{v}{\sqrt{u^2+v^2}} & \frac{-u}{u^2+v^2} \end{pmatrix} \begin{pmatrix} \delta^* sp \\ \delta^* dir \end{pmatrix} \tag{5}$$

2.2 Innovation vector

The innovation vector (IV) is defined as the background minus observation (OMB). The earth-relative *sp* and *dir* observations exist on the same grid coordinate as the background. The background *sp* and *dir* are derived from the model wind vector components. The range of IV_{dir} is defined as [-180, 180], which ensures the *dir* analysis will always fall within as area of smaller absolute value (i.e., 360° ±OMB) when the absolute value of OMB is greater than 180°.

3. Analysis difference between assimilation methods

Two diagrammatic sketches are showed for presenting the differences of analyses between two assimilation methodology. In Fig. 1, if we assume, for the purposes of an idealized example, that the weighting, or error, between the background (fg) and observation (obs) is equal (i.e., $\eta_{fg} = \eta_{obs} = 0.5$), then the analysis vector using the conventional methodology ANA_{asm_uv} will be calculated from components that are halfway between the background and observation: $U_{ANA} = \eta_{fg} U_{fg} + \eta_{obs} U_{obs}$ and $V_{ANA} = \eta_{fg} V_{fg} + \eta_{obs} V_{obs}$. Whereas, the magnitude of the analysis vector for the new methodology, ANA_{asm_wind}, is halfway between sp_{obs} and sp_{fg}, and the direction is the angle midway between the angles dir_{obs} and dir_{fg}.

The obvious differences can be seen between two analyses. It might also be noted that the *dir* of analysis from asm_uv is more sensitive to the observational error of *sp* when the large *dir* difference between background and observation exists. Larger *sp* observational error will lead to the analysis closer to background in the terms of both *sp* and *dir*, and the opposite is right likewise (The conclusion can also be seen in the following OSSE experiment part). The *sp* and *dir* are observed independently, so they have different unrelated sources of error;

thus it is reasonable to assume that the change of *sp* observational error will not impact the *dir* of analysis. Additionally, the magnitude of ANA_{asm_uv} is significant less than both the background and the observation based on this case. The ANA_{asm_uv} is more likely to produce a discontinuity in the flow field because it resides outside of the two best estimations of the true atmosphere.

Implications of this new methodology also apply to the observation selection and rejection criteria. In asm_wind, the quality control process is related to the OMB magnitude and the observational errors of both *sp* and *dir*. However, in asm_uv, a wind observation will be assimilated (rejected) regardless of the magnitude of the *dir* OMB provided the *u* and *v* OMB are smaller (larger) than *n* times the *sp* observational error ($n = 5$ is the WRF default).

Figure 2 presents two cases (ob1, fg1) and (ob2, fg2) where the decision to assimilate or reject an observation will be different based on the method employed. For this example, we assume the wind speed observational error is 2.0 m s^{-1}, and the rejection threshold for OMB is five times the assigned error (i.e., 10 m s^{-1}).

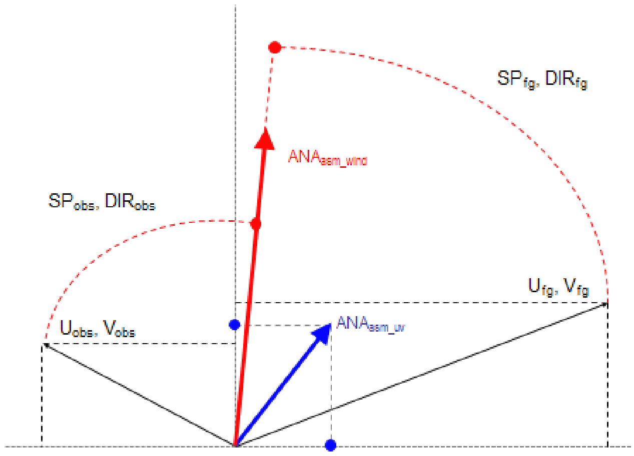

Fig. 1.The difference between the analyses based on the conventional assimilation of vector components (ANA_{asm_uv}) versus wind speed and direction (ANA_{asm_wind}).The vectors (u_{obs}, v_{obs}) and (u_{fg}, v_{fg}) are the observation and background, respectively.

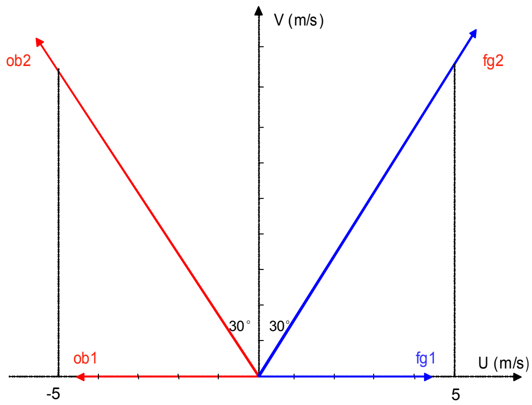

Fig. 2. A schematic diagram for the selection/rejection of observation by case 1 (ob1, fg1) and case 2 (ob2, fg2).

In case 1 (ob1, fg1), if the speed of fg and ob are $\leqslant$ 5 m s^{-1}, the OMB will be $\leqslant$ 10 m s^{-1}. The observation will be assimilated based on the conventional methodology. If the angle difference is large enough like in Fig. 1, the *dir* of analysis will be very sensitive and totally depend on *sp* error (shown in Table 1). In this situation, a regular analysis is less likely to obtain, and the continuity of background may be disrupted. Thus, the new method is a sensible choice to reject this observation based on the OMB *dir*.

In case 2 (ob2, fg2), the speed of fg and ob are both > 10 m s^{-1}, and the angle between them is 60°, thus the OMB_u >10 m s^{-1}. In general situation, the angle between them may be small enough and reasonable to accept for assimilation, but the OMB_u > 10 m s^{-1}, based entirely on the *u* component difference between fg and ob, cannot pass the quality control process in asm_uv. The observation would be rejected (assimilated) based on the conventional (new) methodology. By comparing the differences between case 1 and 2, the advantage of the new methodology is significant when it comes to selecting observations.

Generally, the wind direction observations with low speeds in near-surface levels can be easily affected by the underlying surface, which may cause larger *dir* OMB for asm_wind to reject. In upper levels where jet streams are located, more wind observations with high speeds, often in good quality, are responsible for asm_uv to reject. Typically, the case 1 is more likely to happen in lower levels, and case 2 is in upper levels in the assimilation process. In the following part, a set of OSSE experiments are presented for explaining the advantage of direct assimilation of wind speed and direction.

4. Observing System Simulation Experiments (OSSE)

4.1 Single-observation experiments

It is expected that a similar analysis will be obtained in the case of the same data assimilated by two methods. Figure 3 presents the increments of *u* and *v* components from the assimilation of a single 500hPa wind observation in asm_uv and asm_wind ways. Although *u*/*v* differences with a maximum value of 1.4/1.3 m s^{-1} happen in the magnitude, the similar patterns guarantee there is not obvious abnormal differences between the analyses in asm_uv and asm_wind. However, to be noted, the analysis in asm_wind will change only with the observational error of *dir*.

Table 1 shows the different analyses generated in asm_uv and asm_wind based on the changing observational errors. As shown in Fig. 1, 2, the observational errors of *dir* are considered in asm_wind, so that the *sp* or *dir* of analysis changes only with the corresponding *sp* or *dir* observational errors. As a comparison, the observational error of *dir* doesn't make any sense in asm_uv. The *dir* differences of analyses in asm_uv are totally sourcing from the changing *sp* observation errors. This will cause some problems, especially when some different types of observations exists in the same grid area for assimilation, because it is not necessary for *sp* and *dir* observational errors of any one type of observations to be coinstantaneous less or larger than the observational errors of any other type of observation and background. In addition, the observational errors for *sp* and *dir* often are from different sources. So, that the *sp* observational errors make impacts on *dir* of analyses is not a reasonable theory.

For the situation of the large *dir* difference between the background and observation, the disadvantage of asm_uv is highlighted in Table 2 and Fig. 4. The *sp* differences of analyses are expected with the *sp* observational errors. However, the *dir* is too sensitive to the *sp* observational errors. The extra 114° *dir* difference brings a large enough indeterminacy for *dir* of analysis. Similar to the case in Fig. 1, the *sp* of two analyses both reside outside of background and observations.

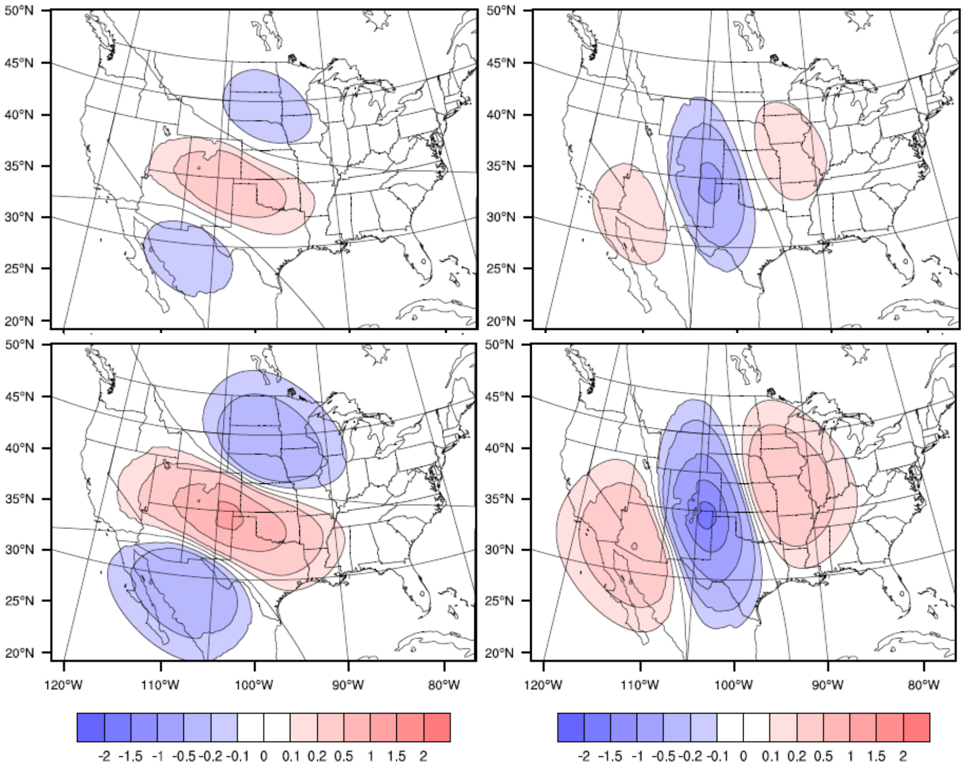

Fig. 3. The 500-hPa *u* (left) and *v* (right) components increments by assimilating a single observation at 500-hPa at (36.5N, 103.6W) in ams_uv (up) and asm_wind (bottom) ways. Case from 00 UTC Dec 16.

Table 1 The comparison of analysis sourcing from new and default methodology

	speed (m/s)	direction (degree)	Sp. Obs. Err (m/s)	Dir. Obs. Err (degree)
Background	6.705	246.320	/	/
Observation	9.705	276.320		
Analysis from asm_wind	7.135	266.225	3	8.5
	7.135	**263.595**	**3**	**10**
	7.135	253.442	3	20
	7.525	263.595	2	10
	7.135	**263.595**	**3**	**10**
	6.964	263.595	4	10
Analysis from asm_uv	7.243	257.830	2	8.5 / 10 / 20
	6.952	**252.550**	**3**	**8.5 / 10 / 20**
	6.843	250.250	4	8.5 / 10 / 20

Corresponding to what the schematic diagrams show (Fig. 1,2), the similar qualitative conclusions are obtained based on the single observation experiments. The asm_wind does make effective impacts on the assimilation process. The following part will show the results from a set of OSSE.

Table 2 A case for the impacts of sp observational error on dir

	speed (m/s)	direction (degree)	Sp. Obs. Err (m/s)	Dir. Obs. Err (degree)
Background	1.93	145.71	/	/
Observation	4.519	301.29		
Analysis from asm_uv	0.804	263.8	1	/
	1.549	150.0	**3**	**/**

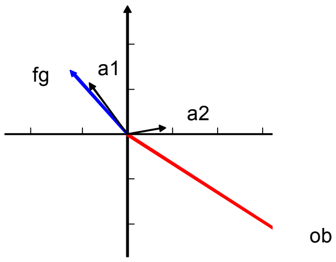

Fig. 4. The analysis by assimilating a single observation at 1007hPa at (36.5N, 103.6W) in ams_uv ways. Case from 00 UTC Dec 16. a1/a2 in right picture are the analyses based on the *sp* observational error of 3m/s / 1m/s, corresponding to Table 2.

4.2 Experiment design for OSSE

As an initial step to test and understand the newly developed assimilation way for the assimilation of wind observation, a set of OSSE is configured that is relatively simple in a controlled and manageable environment. Its advantage is to provide a "nature" run for verification, which is considered a perfect state of atmospheric generated by a numerical prediction model that has a known history calibrated against reality (Hoffman et al. 1990).

An OSSE process typically consists of four components or steps. 1) Generate a “nature” run atmosphere, normally by a higher resolution model, which is as close as possible to the nature for synthetic observations and verification; 2) Compute synthetic observations. The model data is extracted at observation sites and times from the “nature” run, and then random errors are introduced to mimic the observational error; 3) Assimilate the synthetic observations from step 2 and run a set of forecasts based on an independent lower resolution model; and 4) Assess the impacts of the synthesized observations on the resulting forecasts.

Previous studies showed the steady and remarkable forecast scores based on the WRF ARW model (Etherton 2008; Shafer et al. 2010), which built the foundation for this study. In this study, experiments were performed running the WRF model (v3.3) on a domain covering main continental and the surrounding oceans (Fig. 5). The detailed description of the model can be found in Skamarock et al. (2008). The “nature run” is generated based on a 6-km grid spacing with 57 vertical levels and a model top at 50 hPa. Initial and lateral boundary conditions were obtained from NCEP final analysis. The same physics configuration is used as Huang et al.(2009), except the Kain-Fritsch cumulus parameterization (Kain 2004). In view of focusing on an assimilation way, not an observation type, a set of simulated regular observations with a horizontal resolution of 180 km (every 30 grids) and a vertical resolution of 3 eta levels are generated by adding gaussian-distribution error to the model data from the “nature” run. The standard deviation of the random noise of *sp* and *dir* are 3.0 m/s and 30º with zero mean. Then the cycle assimilation and forecast experiments were run using WRF model and WRFDA (v3.3) with a 18 km grid spacing with 43 vertical levels and a model top at 50 hPa. Fig. 5, 6 show a snapshot of the horizontal distribution of the simulated observations and the perturbations for *sp* and *dir* on 00UTC Dec. 17.

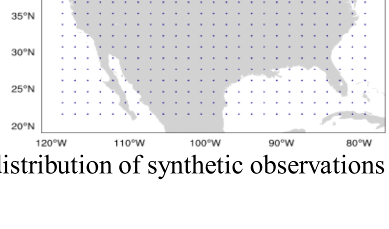

Fig. 5. The horizontal distribution of synthetic observations and experiment domain.

The cycle simulation started at 0000 UTC 16 Dec 2011. Lateral boundary conditions were provided by NCEP GFS forecast. The observations were assimilated in asm_uv and asm_wind ways every 6 h for 24 hr (5 cycle times), and then 24 hr forecast were verified against the "nature" run. The true error is assigned in assimilation experiments.

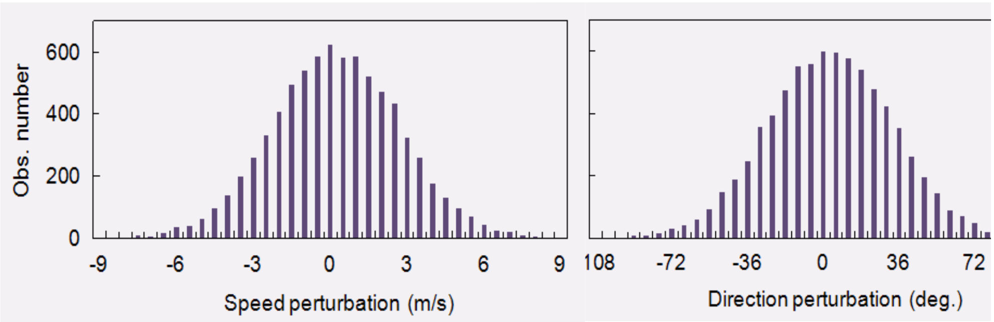

Fig. 6. The perturbations meeting gaussian distribution for *SP* and *DIR* on 00UTC Dec. 17

4.3 The analysis of assimilation process and the verification of forecasts

As discussed above, some observations (e.g., Fig. 2) will lead to main local differences between analyses in two assimilation ways. Figure 7 presents the observation number assimilated in asm_uv and asm_wind ways. Obviously, more observations are assimilated below 800 hPa in asm_uv way, and the opposite is right in higher levels, which is assorted to Fig. 2. The difference of observations assimilated are bound to affect the assimilation process.

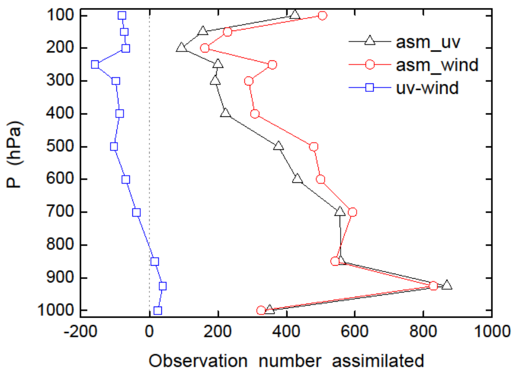

Fig. 7. The total observation number assimilated in asm_uv and asm_wind ways in 5 cycle assimilation times.

The observation minus analysis (OMA) and OMB are two important indexes to monitor the assimilation process. Fig. 8 presents the profile of OMA and OMB of wind speed and direction in asm_uv and asm_wind ways as the average of 5 cycle assimilation times.

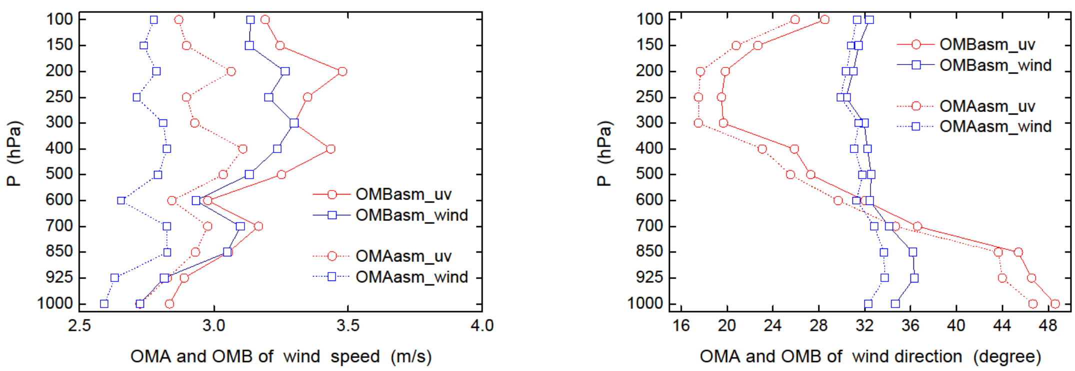

Fig. 8. The OMA and OMB of wind speed and direction analysis in asm_uv and asm_wind

Two major features are clear: 1) OMA are smaller than OMB for both assimilation methods. It shows that the observations make sense in the assimilation process, where the balance is achieved between background and observations in the meaning of cost function minimization. 2) the OMA and OMB in asm_wind are smaller than that in asm_uv for *sp*. For *dir*, corresponding to Fig.2, more observations with large *dir* OMB are assimilated in lower levels in asm_uv, which results in the larger *dir* OMA and OMB. In the upper levels, more observations with large wind speed are rejected by asm_uv, which is the reason why the statistics in asm_uv are smaller. Generally, the smaller OMA will produce an analysis with higher quality, but it also depends on the quality of observations. Although smaller *dir* OMA in asm_uv than that in asm_wind in upper levels, so the better analysis is still from the asm_wind method (Fig. 9).

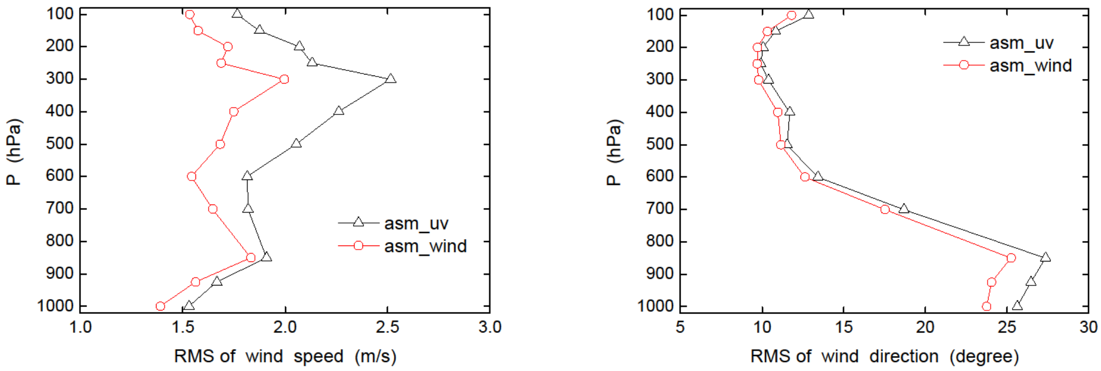

Fig. 9 The profiles of RMS of wind speed and direction analysis in asm_uv and asm_wind

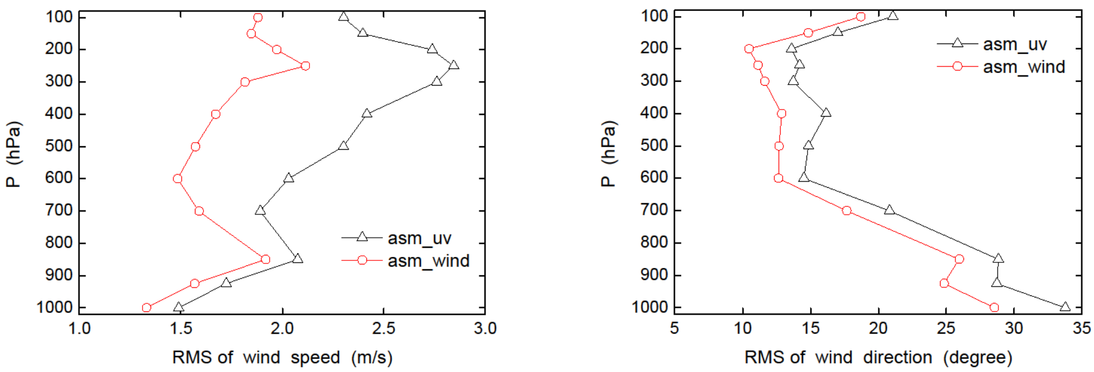

Fig. 10 The profiles of RMS of wind speed and direction forecast in asm_uv and asm_wind

Fig. 10 presents RMS of wind speed and direction forecasts for asm_uv and asm_wind against "nature" within the full domain. After 5 cycle assimilations, where the observation information is accumulated, a better analysis is obtained in asm_wind way for both wind speed and direction, especially for wind speed with the improvement of almost 20% (Fig. 9). The analysis will improve the forecast (Fig. 10), although the improvement of wind direction forecast decreases with forecast time (not shown).

5. Conclusion and outlook

WRFDA 3D-Var assimilation system employs the assimilation of *u* and *v* wind vector components calculated from observed wind speed and direction as the assimilation scheme for wind observations. As a comparison, a new method of directly assimilating wind speed and direction was developed in WRFDA 3D-Var system.

In theory, the wind observation selection, rejection, and weighting wil be more reasonable if the wind direction observational error is considered. The analysis from asm_wind is a continuous function, which can ensure the analysis locates in background and observation in the terms of speed and direction. Asm_wind can reject the pairs with large direction difference which can lead to instability and discontinuous, and save some pairs rejected by ass_uv, which is beneficial.

The single observation experiments conform this theory. The OSSE also shows encouraging results for the new assimilation method. The future plan is to apply the new methodology into real-time runs. It can be expected that the benefit of the new assimilation method may be diminished in real-time implementations by imperfect models, observations with bias, the assimilation of other variables and not so accurate observational error assigned. Actually, the observations in the real-time experiment have a better quality than that in OSSE, which ensure the more similar data assimilated in both methodology; however, the advantage of the theory should produce positive impacts.

References

Courtier, P., J.–N. Thépaut, and A. Hollingsworth, 1994: A strategy for operational implementation of 4D-Var, using an incremental approach. *Quart. J. Roy. Meteor. Soc.*, 120, 1367-1387.

Gao. F., X. Zhang, N. A. Jacobs, X.-Y. Huang, X. Zhang, and P. P. Childs, 2012: Estimation of TAMDAR Observational Error and Assimilation Experiments. Wea. Forecasting, (submitting)

Huang, X.-Y., Q. Xiao, D. M. Barker, Xin Zhang, J. Michalakes, W. Huang, T. Henderson, J. Bray, Y. Chen, Z. Ma, J. Dudhia, Y. Guo, Xiaoyan Zhang, D.-J. Won, H.-C. Lin, Y.-H. Kuo, 2009. Four-Dimensional Variational Data Assimilation for WRF: Formulation and Preliminary Results. Mon. Wea. Rev., 137, 299-314.

Hoffman, R. N., C. Grassotti, R. Isaacs, J. Louis, T. Nehrkorn, and D. Norquist, 1990: Assessment of the impact of simulated satellite lidar wind and retrieved 183 GHz water vapor observations on a global data assimilation system. Mon. Wea. Rev., 118, 2513-2542.

Kain,J. S., 2004: The Kain–Fritsch Convective Parameterization: An Update. *J.Appl.Meteor.*, 43, 170–181.

Etherton, B., P. Santos, 2008: Sensitivity of WRF Forecasts for to Initial Conditions. *Wea. Forecasting,* 23, 725-740.

Parrish, D. F., and J. C. Derber, 1992: The National Meteorological Center's SpectralStatistical Interpolation analysis system. *Mon. Wea. Rev.*, 120, 1747-1763.

Skamarock, W. C., J. B. Klemp, J. Dudhia, D. O. Gill, D. M. Barker, M. Duda, X.-Y. Huang, W. Wang and J. G. Powers, 2008: A Description of the Advanced Research WRF Version 3. NCAR Technical Note, 2008. NCAR/TN–475+STR.

Shafer, C. M., A. E. Mercer, L. M. Leslie, M. B. Richman and C. A. Doswell, 2010: Evaluation of WRF Model Simulations of Tornadic and Nontornadic Outbreaks Occurring in the Spring and Fall. Mon. Wea. Rev., 138, 4098-4119.